nature geoscience

Article

https://doi.org/10.1038/s41561-024-01384-7

Emergent temperature sensitivity of soil organic carbon driven by mineral associations

Received: 23 October 2022

Accepted: 23 January 2024

Published online: 20 February 2024

Check for updates

Katerina Georgiou[1] ✉, Charles D. Koven[2], William R. Wieder[3,4], Melannie D. Hartman[5], William J. Riley[2], Jennifer Pett-Ridge[1,6], Nicholas J. Bouskill[2], Rose Z. Abramoff[2,7], Eric W. Slessarev[1,8], Anders Ahlström[9], William J. Parton[5], Adam F. A. Pellegrini[10], Derek Pierson[11], Benjamin N. Sulman[12], Qing Zhu[2] & Robert B. Jackson[13,14]

Soil organic matter decomposition and its interactions with climate depend on whether the organic matter is associated with soil minerals. However, data limitations have hindered global-scale analyses of mineral-associated and particulate soil organic carbon pools and their benchmarking in Earth system models used to estimate carbon cycle–climate feedbacks. Here we analyse observationally derived global estimates of soil carbon pools to quantify their relative proportions and compute their climatological temperature sensitivities as the decline in carbon with increasing temperature. We find that the climatological temperature sensitivity of particulate carbon is on average 28% higher than that of mineral-associated carbon, and up to 53% higher in cool climates. Moreover, the distribution of carbon between these underlying soil carbon pools drives the emergent climatological temperature sensitivity of bulk soil carbon stocks. However, global models vary widely in their predictions of soil carbon pool distributions. We show that the global proportion of model pools that are conceptually similar to mineral-protected carbon ranges from 16 to 85% across Earth system models from the Coupled Model Intercomparison Project Phase 6 and offline land models, with implications for bulk soil carbon ages and ecosystem responsiveness. To improve projections of carbon cycle–climate feedbacks, it is imperative to assess underlying soil carbon pools to accurately predict the distribution and vulnerability of soil carbon.

Soil carbon–climate feedbacks represent a major uncertainty in the response of the terrestrial biosphere to climate change[1]. This uncertainty stems, in part, from poorly constrained relationships between the temperature sensitivities of the decomposition and stabilization processes of soil organic carbon (C), which are key parameters in soil biogeochemical models[2,3]. Whereas many empirical and modelling studies have explored the effects of temperature on bulk soil C stocks and turnover rates at ecosystem to global scales[4–7], they largely ignore heterogeneity in soil organic matter. This is a key oversight given that underlying soil organic matter fractions or 'pools' (for example, particulate or mineral-associated organic matter) can exhibit different responses to warming in laboratory- and field-based manipulations[8–11].

A full list of affiliations appears at the end of the paper. ✉e-mail: georgiou1@llnl.gov

https://doi.org/10.1038/s41561-024-01384-7

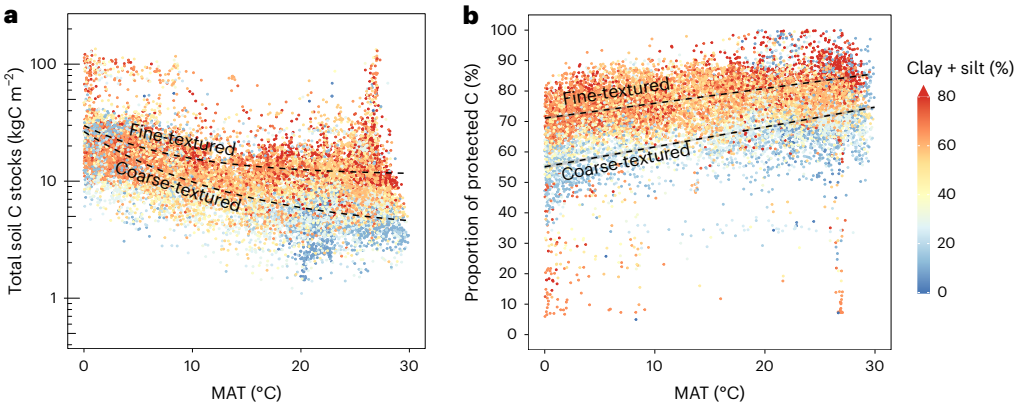

Fig. 1 | Global distribution of observationally derived soil C stocks as a function of climatological temperature and clay and silt minerals. a,**b**, Total soil C stocks (**a**) and the proportion of total soil C that is protected (mineral-associated) (**b**) as a function of the mean annual temperature (MAT) globally. Each gridcell is coloured by the percentage of clay and silt minerals, and best-fit trends are depicted for fine- and coarse-textured soils; here, fine-textured soils were classified as those with >70% clay + silt content and coarse-textured soils with <20% clay + silt content.

Understanding and quantifying the temperature sensitivity of these underlying pools at the global scale is thus critical for accurately predicting emergent feedbacks and soil organic C vulnerabilities to a changing climate.

Warmer soil temperatures accelerate the rate of organic matter decomposition, often leading to losses in bulk soil C stocks[3,5,8,12]. However, the potential decomposability of organic matter in a given soil can depend on its association with minerals[11,13,14]. Mineral-associated organic matter consists of small plant- or microbial-derived monomers and biopolymers that are chemically or physically bound to clay- and silt-sized minerals, whereas particulate organic matter is largely comprised of coarser, partially decomposed fragments of plant material[15,16]. Mineral associations can limit access of microbial constituents and their enzymes to organic matter, and as a result, mineral-associated C is often older than particulate C[16–18]. In soil biogeochemical models, these pools can be represented explicitly[19–22] or implicitly[22–24] (see 'Model pool interpretability' in the Methods), with implications for their transient dynamics and long-term response to novel conditions. For consistency across the data and models, we refer to mineral-associated C (and slowest-cycling pools) as 'protected' and particulate C (and all other model pools) as 'unprotected', while acknowledging that the bioavailability and persistence of each pool is more complex in practice[25]. Importantly, much uncertainty remains in the responses of protected and unprotected soil C to warming across broad spatial scales[9], hindering model benchmarking efforts.

Evaluating the transient dynamics of soil biogeochemical models to warming remains a challenge, in part because observations of soil C at multi-decadal to centennial timescales are limited[26,27]. Laboratory incubations and field studies demonstrate that decomposition rates increase, and C stocks often decrease, with warming[5,8,11]. However, at multi-decadal timescales, acclimatory responses in microbial activity may limit the effect of warming on decomposition rates[26,28]. Furthermore, many experiments focus on the response of bulk soil C stocks, and neither measure nor report the relative responses of underlying soil C fractions. Given these data limitations, an alternative approach is to benchmark global models using spatial gradients[4,29,30]—although this approach is insufficient for constraining transient dynamics (that is, space-for-time assumptions)[31,32], climate gradients do reflect long-term climatological temperature sensitivities that should, in principle, be captured by soil C models.

Here we assess the climatological temperature sensitivity of bulk soil C stocks, and the role of mineral-associated and particulate soil C pools in driving this emergent property in data and models. We first leverage a globally gridded data product of mineral-associated and particulate soil C (derived from an observational synthesis of soil fractions[33]) to quantify the distribution of soil organic C between these two pools and their respective climatological temperature sensitivities at the global scale. We then evaluate the distributions and temperature sensitivities of protected (mineral-associated-like) and unprotected (particulate-like) soil C stocks across an ensemble of 12 global models—namely, nine Earth system models (ESMs) from the Coupled Model Intercomparison Project Phase 6 (CMIP6)[34] and three offline land models[23], including two microbially explicit soil C models (Supplementary Tables 1–3). Although there are important considerations regarding the interpretability of modelled pools and measured fractions (see 'Model pool interpretability' in the Methods), pool-specific benchmarks offer a critical opportunity to refine model formulations and reduce uncertainties. We argue that resolving the distribution and temperature sensitivities of underlying soil C pools is imperative for developing a predictive understanding of the emergent temperature dependence of bulk soil C decomposition and constraining global biogeochemical models.

Climatological temperature sensitivity of soil carbon pools

Soil organic C stocks are known to broadly decrease with increasing temperature across climate gradients[4,30,35]. However, the magnitude of this climatological temperature sensitivity can vary across soils[29]. Indeed, this relationship appears to be modulated by clay and silt content, where fine-textured soils (that is, soils containing higher amounts of clay and silt minerals) have a lower climatological temperature sensitivity compared with coarse-textured sandy soils (inferred from the relative strengths of relationships in Fig. 1a). These contrasting temperature sensitivities can be attributed in part to the mineralogical capacity of each soil[29,36], but more specifically to its effect on the distribution of soil C among mineral-associated and particulate C pools. Since mineral-associated C often has a lower temperature sensitivity than particulate C[2,9,14,37], the proportion of C that is mineral-associated can play a dominant role in driving the emergent bulk soil temperature sensitivity (see conceptual schematic in Supplementary Fig. 1).

Globally, our results indicate that the proportion of soil C that is mineral-associated (hereafter termed 'protected' for consistency with model pools[22,23]) increases with increasing mean temperature (Fig. 1b; a trend that is not captured in most global models (Supplementary Figs. 2 and 3)). Furthermore, fine-textured soils have greater proportions of protected C than do coarse-textured soils across all temperatures. We therefore expect fine-textured soils to exhibit a lower climatological temperature sensitivity compared with coarse-textured sandy

https://doi.org/10.1038/s41561-024-01384-7

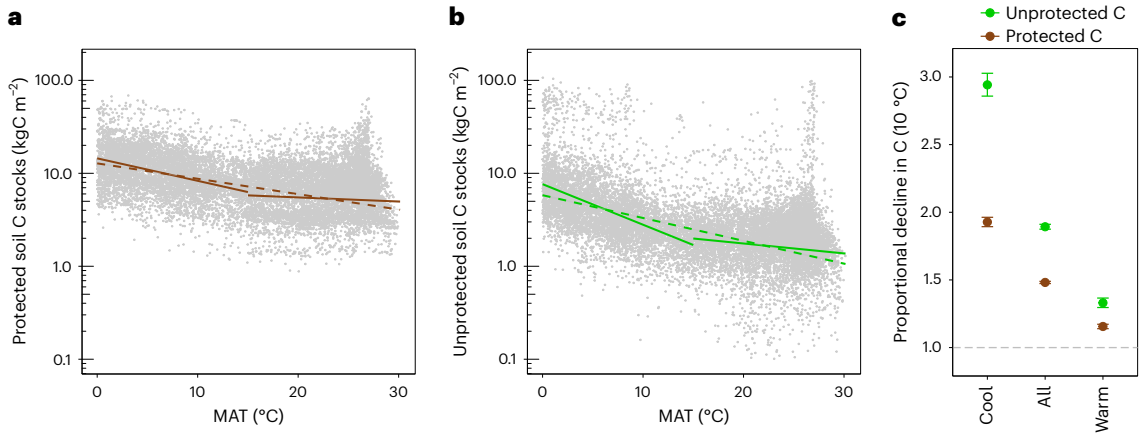

Fig. 2 | Global distribution of observationally derived protected and unprotected soil C stocks as a function of climatological temperature. **a**,**b**, Protected (mineral-associated) (**a**) and unprotected (particulate) (**b**) soil C stocks as a function of MAT in regions above 0 °C globally. Linear regressions are shown for cool (<15 °C) and warm (≥15 °C) regions (solid lines) and across all temperatures above 0 °C (dashed lines). **c**, Climatological temperature sensitivity calculated as the proportional decline of each soil C pool for a 10 °C increase in MAT (analogous to a climatological Q_{10}, but for C stocks) while accounting for potential confounding variables (see 'Data analysis' in the Methods). Points depict the proportional decline of each soil C pool (derived from the regression slopes; n = 32,528 gridcells for non-permafrost mineral soils above 0 °C globally, with n = 13,410 in cool regions and n = 19,118 in warm regions), and error bars denote the 95% CIs (Supplementary Table 6). Higher values (>1) indicate greater decreases in C with increasing climatological temperature.

soils where higher unprotected C stocks drive a higher temperature sensitivity. The climatological temperature sensitivity of bulk soil C emerges from the underlying pool distributions and their respective temperature dependencies.

To assess the climatological temperature sensitivity of each soil C pool, we calculated the proportional decline in C stocks for every 10 °C increase in mean temperature while controlling for potential confounding factors that include primary productivity, precipitation, and clay and silt content (Methods). Our approach builds upon previous studies[29] and provides a benchmarking metric analogous to a climatological Q_{10} (that is, the increase in process rates for each 10 °C increase in temperature) but for C stocks instead of respiration or turnover rates[4,6]. We find that, at the global scale, unprotected C stocks have a 28% (95% confidence interval (CI): 26, 30%) greater climatological temperature sensitivity than protected C stocks (Fig. 2). This pattern is especially pronounced in cool regions (<15 °C) where unprotected C is 53% (46, 60%) more temperature sensitive than protected C, compared with warm regions (≥15 °C) where the relative difference is only 15% (11, 20%). Both soil C pools show weak climatological temperature sensitivities in warm regions (Fig. 2c). This latter result suggests that decomposition in cool regions is more temperature-limited, and that warm regions do not experience as stark a decline in soil C for a given increase in mean temperature. This difference is supported by gradient studies in tropical soils[38,39], and is consistent with incubation studies showing that warm-adapted microbial communities typically show lower temperature sensitivities (namely, Q_{10}) and higher microbial growth efficiencies[40]. Furthermore, warm regions contain higher proportions of protected C (Fig. 1b), such that the emergent bulk soil C temperature sensitivity more closely mirrors that of the protected C pool. Therefore, the proportion of protected C—in addition to its climatological temperature sensitivity—may serve as an important benchmark for evaluating global models.

Global patterns in soil carbon pools across data and models

Soil C models vary in their underlying assumptions, mathematical representations and parameterizations. However, several studies have proposed that the slowest-cycling ('passive') pool of soil C in many ESMs corresponds broadly to mineral-associated (protected) C[15,22–24]. This reflects a common conceptualization of donor-pool sources, mineralogical controls, turnover times and stoichiometry of protected C that are used to approximate the formation and characteristics of mineral-associated organic matter (see 'Model pool interpretability' in the Methods). We thus adopt this convention here, while recognizing that there are still inherent uncertainties in the interpretability of modelled pools and operationally defined fractions. We posit that benchmarks based on relative pool distributions, in tandem with radiocarbon ages[41,42], will be critical for refining future model parameterizations and constraining transient dynamics.

Global soil C models are typically benchmarked on the basis of bulk soil C metrics[43,44]. However, even models that predict similar bulk soil C stocks can vary widely in their underlying pool distributions (Supplementary Fig. 4). Whereas bulk soil C stocks in non-permafrost mineral soils vary 2.5-fold across the CMIP6 ESMs and offline land models in this study, protected soil C stocks vary nearly sevenfold. As a result, the proportion of protected C ranges from 16 to 85% across the global models (Fig. 3 and Supplementary Table 4). This large spread in model predictions presents a critical opportunity to apply data-driven constraints and reduce uncertainty. We find that about half of the analysed ESMs underestimate the proportion of protected C in soils globally compared with the observationally derived data product, and consequently, contain too much C in faster-cycling, unprotected C pools. This result is especially true in non-permafrost mineral soils, where several of the global models underestimate the proportion of protected C in both cool and warm regions (Supplementary Fig. 5 and Supplementary Table 5). In particular, six models (CESM2, CNRM-ESM2-1, E3SM-1-1-ECA, IPSL-CM6A-LR, NorESM2 and the microbially explicit model CORPSE) roughly capture the proportion of protected C, whereas the other six models (ACCESS-ESM1-5, BCC-CSM2-MR, MIROC-ES2L, MRI-ESM2-0, CASA-CNP and the microbially explicit model MIMICS) considerably underestimate this proportion (Fig. 3d). However, we note that all of the models in this study are amenable to matching pool-specific constraints in future work—indeed, both first-order and microbially explicit formulations with refined parameterizations have been able to better match observations in past studies[42,45–47]. Nevertheless, our results generally suggest that soil C is skewed towards faster-cycling C pools in several global models, consistent with radiocarbon-based benchmarking studies that have shown that current ESMs underestimate the mean age of soil C across latitudes[41,42].

https://doi.org/10.1038/s41561-024-01384-7

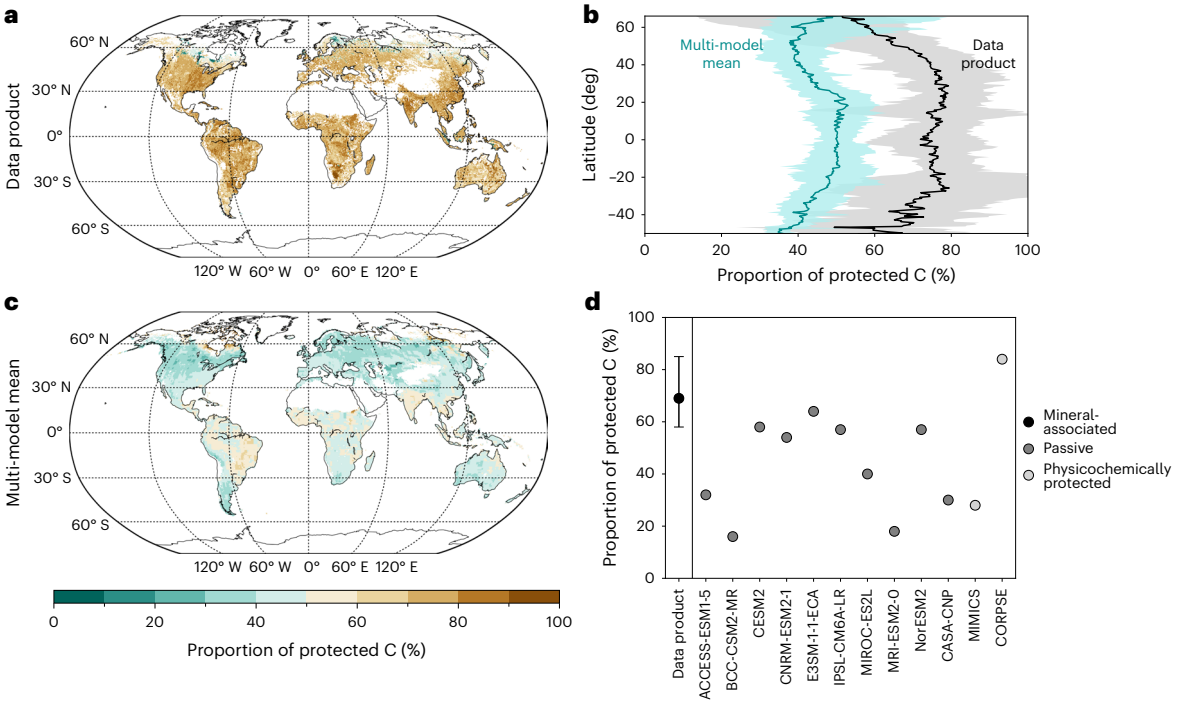

Fig. 3 | Proportion of soil C in protected pools globally across data and models. a–**c**, The percentage of total soil C that is protected in the observationally derived data product and in the multi-model mean of the ensemble of CMIP6 ESMs and offline land models, shown globally (**a**,**c**) and as latitudinal means (**b**; solid lines). Shaded uncertainty ranges in **b** correspond to 90% prediction intervals for the data product[33], and 5th and 95th quantiles of the multi-model ensemble across each latitudinal band. **d**, The global percentage of total soil C that is protected across the individual ESMs and offline land models. Protected C was estimated as the mineral-associated fraction for the data product, physicochemically protected pools in MIMICS and CORPSE, and the slowest-cycling passive pool in the CMIP6 ESMs and CASA-CNP (see 'Model pool interpretability' in the Methods). Global means are given for non-permafrost mineral soils, excluding tundra, deserts and peatlands (n = 39,620 gridcells for 0.5° resolution), and the data product uncertainty range corresponds to the 90% prediction interval[33] (summarized in Supplementary Table 5).

At higher latitudes, the two microbially explicit models depict a lower proportion of protected C (Supplementary Fig. 4), consistent with recent studies[3,14,15,45]. The observationally derived data product also supports this latitudinal trend (Fig. 3b). By contrast, several CMIP6 models show a larger proportion of protected C at higher latitudes (particularly above 0 °C; Supplementary Fig. 3), which suggests that the interpretability of the protected pool as mineral-associated may break down in these regions within certain CMIP6 models. For instance, in models with vertically resolved soil biogeochemistry (CESM2, E3SM-1-1-ECA and NorESM2) these larger proportions of protected C may be caused by the relative timescales of decomposition and vertical mixing processes. This is because high-latitude active-layer C is transported to permafrost layers via a slow constant diffusion rate representing cryoturbation[48,49], which consequently transports a greater fraction of slower-cycling C relative to fast-cycling C pools. Whereas soil C is indeed old in these high latitudes[41], its decomposition is limited more by low temperatures that reduce the availability of liquid water than by association with minerals[4,50]. Given that temperature and hydrology can change at decadal timescales, representing long-lived organic matter at high latitudes as an inherently slow-cycling pool (as opposed to unprotected, particulate forms that can be more sensitive to disturbance[9,11,13]) has important implications for the responsiveness of vast permafrost soil C pools to projected climate change (Supplementary Figs. 6–8).

Temperature sensitivity of soil carbon in global models

The climatological temperature sensitivity of bulk soil C is an emergent property that ultimately depends on the distribution of C within underlying pools and their respective temperature sensitivities. Whereas some models may appear to capture the observationally derived climatological temperature sensitivity of bulk soil C stocks, this agreement does not always occur for the right reasons and may break down when considering the contribution of underlying protected and unprotected soil C pools. For example, six of the CMIP6 ESMs (ACCESS-ESM1-5, CESM2, CNRM-ESM2-1, E3SM-1-1-ECA, IPSL-CM6A-LR and NorESM2) and two microbially explicit models (MIMICS and CORPSE) roughly capture the temperature sensitivity of bulk soil C stocks (Fig. 4 and Supplementary Table 6). However, these same models show divergent distributions and climatological temperature sensitivities of underlying protected and unprotected soil C pools (Fig. 4). Only a few models roughly capture the climatological temperature sensitivity of protected C (CESM2, CNRM-ESM2-1, IPSL-CM6A-LR, NorESM2 and CORPSE) and even fewer of unprotected C (ACCESS-ESM1-5, MIMICS and CORPSE).

The observationally derived data product broadly suggests that protected C has a lower climatological temperature sensitivity than unprotected C (Fig. 2). The models generally agree with this trend, although the difference in climatological temperature sensitivities of pools is less pronounced in the CMIP6 models than in the microbially explicit models (Fig. 4). This difference may arise because many first-order soil models impose the same temperature-dependence parameters across all pools[49,51], and consequently the emergent climatological temperature sensitivities are often similar between pools. There are a few notable exceptions among the CMIP6 models, in which unprotected C appears less temperature sensitive than protected C (namely, MRI-ESM2-0 and to a lesser degree E3SM-1-1-ECA (Fig. 4), as well as CESM2, CNRM-ESM2-1, MIROC-ES2L and NorESM in cool regions (Supplementary Fig. 9)). This could arise due to temperature-sensitivity parameterizations based on a presumed greater molecular complexity

https://doi.org/10.1038/s41561-024-01384-7

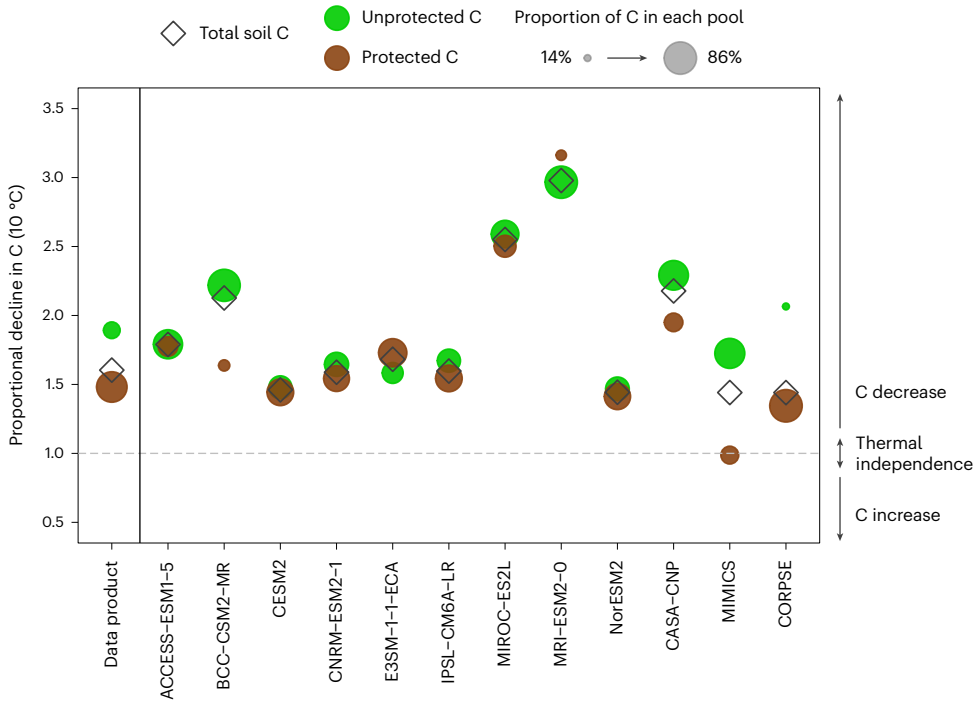

Fig. 4 | Climatological temperature sensitivity of total soil C and the contribution of protected and unprotected pools. The climatological temperature sensitivity of total soil C (denoted by a diamond) is an emergent property of the climatological temperature sensitivity of protected (brown circles) and unprotected (green circles) soil C pools, as well as the proportion of C within each of these pools (denoted by the marker area). The proportional decline in C for a 10 °C increase in MAT was calculated for each C pool, controlling for potential confounding variables (see 'Data analysis' in the Methods). Results are shown for the data product and an ensemble of ESMs and offline land models across gridcells with MAT > 0 °C globally; 95% CIs are given in Supplementary Table 6. Higher values (>1) indicate greater decreases in C with increasing climatological temperature, lower values (<1) indicate increases in C and values equal to 1 (grey dashed line) indicate thermal independence.

of protected C in select models[2,10]. Ultimately, the distinct climatological temperature sensitivities of underlying soil C pools observed in the data product and process-based models can have important implications for transient projections, especially with regard to C ages and ecosystem responsiveness, and constitute an important benchmark for evaluating model performance.

Since protected C makes up the majority of bulk soil C globally in the data product (Fig. 3d), it also dominates the climatological temperature sensitivity of bulk soil C stocks (Fig. 4). However, many models do not capture this pattern. In fact, unprotected C dominates the bulk soil C stocks and climatological temperature sensitivity in a few models (BCC-CSM2-MR, MRI-ESM2-0, CASA-CNP and MIMICS), whereas most other ESMs have similar proportions and temperature sensitivities of underlying C pools. Only a couple of global models have high enough proportions of protected C to drive bulk climatological temperature sensitivities that are dominated by the protected C pool (for example, E3SM-1-1-ECA and CORPSE), as observed in the data product (Fig. 4 and Supplementary Fig. 9).

Furthermore, climatological temperature sensitivities of bulk soil C stocks and turnover can vary across climates, where temperature dependencies are typically higher in cooler climates than in warmer climates[4,29,52]. However, the temperature sensitivities of underlying soil C pools within these climate regimes have not been explored in global-scale models or observations. We find that both protected and unprotected C pools show greater climatological temperature sensitivities in cool than warm climates, but interestingly, this contrast across climates is more pronounced for unprotected C than for protected C, and especially in the observationally derived data product compared with the global models (Figs. 2 and 5 and Supplementary Figs. 9–11).

Overall, our analysis shows that global models tend to overestimate the climatological temperature sensitivity of protected C stocks in both cool and warm climates, and of both C pools in warm climates (Fig. 5). This is especially true of MIROC-ES2L, CASA-CNP and MRI-ESM2-0, which overestimate the climatological sensitivity of protected C by more than a factor of two. However, the global models tend to underestimate the climatological temperature sensitivity of unprotected C in cool climates (Fig. 5). The inability of most ESMs to match these regional patterns suggests that the transient response to warming may also be biased, particularly in cool climates. Protected (slower-cycling) C in ESMs may be overly sensitive to warming in cool regions, whereas unprotected (faster-cycling) C may not be sensitive enough to warming, with implications on soil C dynamics and age distributions under future scenarios.

Implications and future perspectives

We propose that the distributions and climatological temperature sensitivities of underlying soil C pools are ecosystem properties that global models should be expected to reproduce. Our results highlight that even ESMs that predict similar bulk soil C stocks and climatological temperature sensitivities can vary widely in their predictions of underlying soil C pools, with implications for C ages and ecosystem responsiveness under changing conditions. In particular, owing to an overestimation of C in unprotected (faster-cycling) pools, several CMIP6 ESMs may be too responsive to C inputs and may overestimate the effects of increased primary production on potential soil C sequestration (for example, with large increases in unprotected C; Supplementary Fig. 6); a finding that agrees with independent radiocarbon-based studies[41,42]. This implies that model estimates of the amount of C sequestration that may result from climate change and CO_2 fertilization of terrestrial ecosystems may be too strong. Furthermore, most ESMs tend to underestimate the climatological temperature sensitivity of unprotected C in cool climates, potentially leading to an underestimation of C losses from

https://doi.org/10.1038/s41561-024-01384-7

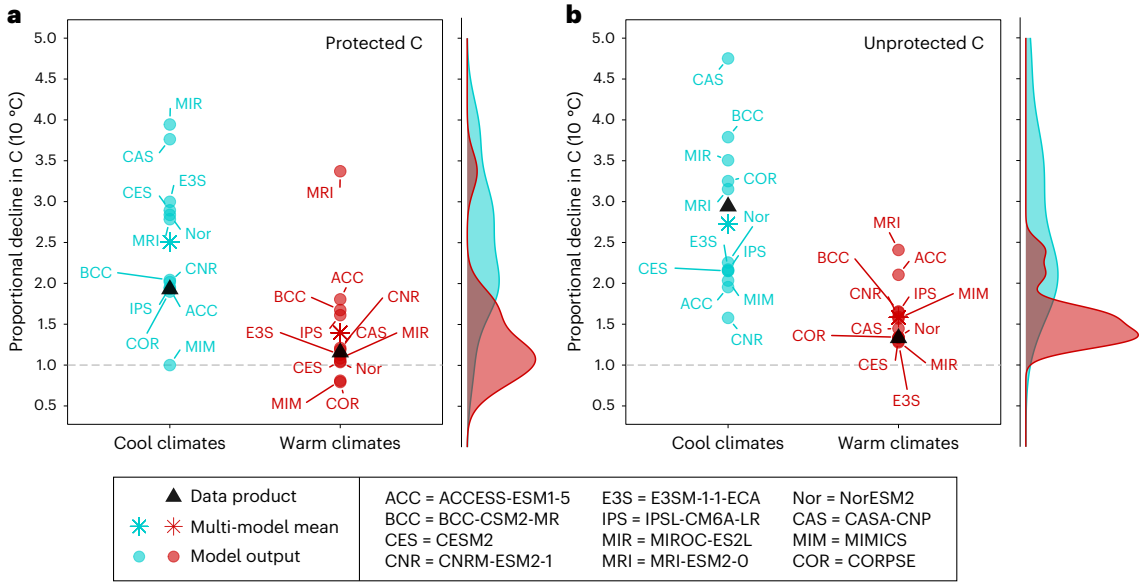

Fig. 5 | Climatological temperature sensitivity of protected and unprotected soil C across temperature regimes. a,**b**, The proportional decline in protected (**a**) and unprotected (**b**) soil C stocks for a 10 °C increase in MAT, controlling for potential confounding variables. Proportional declines are shown for cool climates (0 °C < MAT < 15 °C; blue circles) and warm climates (MAT ≥ 15 °C; red circles). Results are shown for the data product (black triangles), the multi-model ensemble mean (asterisks) and each ESM and offline land model (solid circles; labelled with abbreviations); 95% CIs are given in Supplementary Table 6. Kernel density estimates are shown for each panel, illustrating the distribution of climatological temperature sensitivities across the model ensemble for each pool and temperature regime. Higher values (>1) indicate greater decreases in C with increasing climatological temperature, lower values (<1) indicate increases in C and values equal to 1 (grey dashed line) indicate thermal independence.

these unprotected pools with warming, an underestimation of the global carbon cycle–climate feedback and compounding projections of higher productivity-driven C accumulation in these regions. Whereas this bias may be partially offset in ESMs that overestimate the climatological temperature sensitivity of protected C across climates, the effect of this latter overestimate on projections of carbon cycle–climate feedbacks is probably weaker because these pools are intrinsically slow-cycling in first-order soil models and consequently change very little on timescales relevant to climate policy (Supplementary Figs. 6–8). Divergent pool-specific responses can ultimately lead to differences in soil C composition and functioning. It is therefore imperative that models benchmark not only bulk climatological sensitivities but also those of underlying soil C pools, to confidently project soil C dynamics into the future.

The CMIP protocol requests but does not require the reporting of soil C pool distributions[53], and, thus, this information is currently available only for a subset of CMIP6 ESMs. Our results show that, with recent advances in global estimates of protected and unprotected soil C stocks[33], redefining and benchmarking these underlying soil C pools can serve as an important constraint for ESMs. We therefore urge that all global models report the distribution of soil C among underlying pools in CMIP Phase 7 and beyond, so that future studies may leverage this benchmark for model evaluation across climate gradients. Although further study of transient responses is also imperative for constraining dynamic models[31,54], the static relationships presented here serve as important benchmarks of long-term temperature effects on the formation and decomposition of soil C pools.

Online content

Any methods, additional references, Nature Portfolio reporting summaries, source data, extended data, supplementary information, acknowledgements, peer review information; details of author contributions and competing interests; and statements of data and code availability are available at https://doi.org/10.1038/s41561-024-01384-7.

References

1. Friedlingstein, P. et al. Uncertainties in CMIP5 climate projections due to carbon cycle feedbacks. *J. Clim.* **27**, 511–526 (2014).
2. Davidson, E. A. & Janssens, I. A. Temperature sensitivity of soil carbon decomposition and feedbacks to climate change. *Nature* **440**, 165–173 (2006).
3. García-Palacios, P. et al. Evidence for large microbial-mediated losses of soil carbon under anthropogenic warming. *Nat. Rev. Earth Environ.* **2**, 507–517 (2021).
4. Koven, C. D., Hugelius, G., Lawrence, D. M. & Wieder, W. R. Higher climatological temperature sensitivity of soil carbon in cold than warm climates. *Nat. Clim. Chang.* **7**, 817–822 (2017).
5. Crowther, T. et al. Quantifying global soil C losses in response to warming. *Nature* **104**, 104–108 (2016).
6. Todd-Brown, K., Zheng, B. & Crowther, T. W. Field-warmed soil carbon changes imply high 21st-century modeling uncertainty. *Biogeosciences* **15**, 3659–3671 (2018).
7. Van Gestel, N. et al. Predicting soil carbon loss with warming. *Nature* **554**, E4–E5 (2018).
8. Hicks Pries, C. E., Castanha, C., Porras, R. & Torn, M. S. The whole-soil carbon flux in response to warming. *Science* **355**, 1420–1423 (2017).
9. Rocci, K. S., Lavallee, J. M., Stewart, C. E. & Cotrufo, M. F. Soil organic carbon response to global environmental change depends on its distribution between mineral-associated and particulate organic matter: a meta-analysis. *Sci. Total Environ.* **793**, 148569 (2021).
10. Conant, R. T. et al. Temperature and soil organic matter decomposition rates – synthesis of current knowledge and a way forward. *Glob. Chang. Biol.* **17**, 3392–3404 (2011).
11. Soong, J. L. et al. Five years of whole-soil warming led to loss of subsoil carbon stocks and increased CO_2 efflux. *Sci. Adv.* **7**, eabd1243 (2021).

12. Nottingham, A. T., Meir, P., Velasquez, E. & Turner, B. L. Soil carbon loss by experimental warming in a tropical forest. *Nature* **584**, 234–237 (2020).
13. Pellegrini, A. F. A. et al. Low-intensity frequent fires in coniferous forests transform soil organic matter in ways that may offset ecosystem carbon losses. *Glob. Chang. Biol.* **27**, 3810–3823 (2021).
14. Lugato, E., Lavallee, J. M., Haddix, M. L., Panagos, P. & Cotrufo, M. F. Different climate sensitivity of particulate and mineral-associated soil organic matter. *Nat. Geosci.* **14**, 295–300 (2021).
15. Sokol, N. W. et al. Global distribution, formation and fate of mineral-associated soil organic matter under a changing climate: a trait-based perspective. *Funct. Ecol.* **36**, 1411–1429 (2022).
16. Lavallee, J. M., Soong, J. L. & Cotrufo, M. F. Conceptualizing soil organic matter into particulate and mineral-associated forms to address global change in the 21st century. *Glob. Chang. Biol.* **26**, 261–273 (2020).
17. Kögel-Knabner, I. et al. Organo-mineral associations in temperate soils: integrating biology, mineralogy, and organic matter chemistry. *J. Plant Nutr. Soil Sci.* **171**, 61–82 (2008).
18. Heckman, K. et al. Beyond bulk: density fractions explain heterogeneity in global soil carbon abundance and persistence. *Glob. Chang. Biol.* **28**, 1178–1196 (2022).
19. Wieder, W. R., Allison, S. D., Davidson, E. A., Georgiou, K. & Hararuk, O. Explicitly representing soil microbial processes in Earth system models. *Glob. Biogeochem. Cycles* **29**, 1782–1800 (2015).
20. Sulman, B. N., Phillips, R. P., Oishi, A. C., Shevliakova, E. & Pacala, S. W. Microbe-driven turnover offsets mineral-mediated storage of soil carbon under elevated CO_2. *Nat. Clim. Chang.* **4**, 1099–1102 (2014).
21. Ahrens, B., Braakhekke, M. C., Guggenberger, G., Schrumpf, M. & Reichstein, M. Contribution of sorption, DOC transport and microbial interactions to the ^{14}C age of a soil organic carbon profile: Insights from a calibrated process model. *Soil Biol. Biochem.* **88**, 390–402 (2015).
22. Sulman, B. N. et al. Multiple models and experiments underscore large uncertainty in soil carbon dynamics. *Biogeochemistry* **141**, 109–123 (2018).
23. Wieder, W. R., Sulman, B. N., Hartman, M. D., Koven, C. D. & Bradford, M. A. Arctic soil governs whether climate change drives global losses or gains in soil carbon. *Geophys. Res. Lett.* **46**, 14486–14495 (2019).
24. Berardi, D. et al. 21st-century biogeochemical modeling: challenges for Century-based models and where do we go from here? *Glob. Chang. Biol. Bioenergy* **12**, 774–788 (2020).
25. Kleber, M. et al. Dynamic interactions at the mineral–organic matter interface. *Nat. Rev. Earth Environ.* **2**, 402–421 (2021).
26. Melillo, J. M. et al. Long-term pattern and magnitude of soil carbon feedback to the climate system in a warming world. *Science* **358**, 101–105 (2017).
27. Walker, T. W. N. et al. A systemic overreaction to years versus decades of warming in a subarctic grassland ecosystem. *Nat. Ecol. Evol.* **4**, 101–108 (2020).
28. Bradford, M. Thermal adaptation of decomposer communities in warming soils. *Front. Microbiol.* **4**, 333 (2013).
29. Hartley, I. P., Hill, T. C., Chadburn, S. E. & Hugelius, G. Temperature effects on carbon storage are controlled by soil stabilisation capacities. *Nat. Commun.* **12**, 6713 (2021).
30. Doetterl, S. et al. Soil carbon storage controlled by interactions between geochemistry and climate. *Nat. Geosci.* **8**, 780–783 (2015).
31. Abramoff, R. Z., Torn, M. S., Georgiou, K., Tang, J. & Riley, W. J. Soil organic matter temperature sensitivity cannot be directly inferred from spatial gradients. *Glob. Biogeochem. Cycles* **33**, 761–776 (2019).
32. Luo, Z. et al. Convergent modelling of past soil organic carbon stocks but divergent projections. *Biogeosciences* **12**, 4373–4383 (2015).
33. Georgiou, K. et al. Global stocks and capacity of mineral-associated soil organic carbon. *Nat. Commun.* **13**, 3797 (2022).
34. Eyring, V. et al. Overview of the Coupled Model Intercomparison Project Phase 6 (CMIP6) experimental design and organization. *Geosci. Model Dev.* **9**, 1937–1958 (2016).
35. Jobbágy, E. G. & Jackson, R. B. The vertical distribution of soil organic carbon and its relation to climate and vegetation. *Ecol. Appl.* **10**, 423–436 (2000).
36. Ahrens, B. et al. Combination of energy limitation and sorption capacity explains ^{14}C depth gradients. *Soil Biol. Biochem.* **148**, 107912 (2020).
37. Gentsch, N. et al. Temperature response of permafrost soil carbon is attenuated by mineral protection. *Glob. Chang. Biol.* **24**, 3401–3415 (2018).
38. Giardina, C. P. & Ryan, M. G. Evidence that decomposition rates of organic carbon inmineral soil do not vary with temperature. *Nature* **404**, 858–861 (2000).
39. Giardina, C. P., Litton, C. M., Crow, S. E. & Asner, G. P. Warming-related increases in soil CO_2 efflux are explained by increased below-ground carbon flux. *Nat. Clim. Chang.* **4**, 822–827 (2014).
40. Wang, C. et al. The temperature sensitivity of soil: microbial biodiversity, growth, and carbon mineralization. *ISME J.* **15**, 2738–2747 (2021).
41. Shi, Z. et al. The age distribution of global soil carbon inferred from radiocarbon measurements. *Nat. Geosci.* **13**, 555–559 (2020).
42. He, Y. et al. Radiocarbon constraints imply reduced carbon uptake by soils during the 21st century. *Science* **353**, 1419–1424 (2016).
43. Todd-Brown, K. E. O. et al. Causes of variation in soil carbon simulations from CMIP5 Earth system models and comparison with observations. *Biogeosciences* **10**, 1717–1736 (2013).
44. Ito, A. et al. Soil carbon sequestration simulated in CMIP6-LUMIP models: implications for climatic mitigation. *Environ. Res. Lett.* **15**, 124061 (2019).
45. Abramoff, R. Z. et al. Improved global-scale predictions of soil carbon stocks with Millennial Version 2. *Soil Biol. Biochem.* **164**, 108466 (2022).
46. Zimmermann, M., Leifeld, J., Schmidt, M. W. I., Smith, P. & Fuhrer, J. Measured soil organic matter fractions can be related to pools in the RothC model. *Eur. J. Soil Sci.* **58**, 658–667 (2007).
47. Pierson, D. et al. Optimizing process-based models to predict current and future soil organic carbon stocks at high-resolution. *Sci. Rep.* **12**, 10824 (2022).
48. Koven, C. et al. On the formation of high-latitude soil carbon stocks: effects of cryoturbation and insulation by organic matter in a land surface model. *Geophys. Res. Lett.* https://doi.org/10.1029/2009GL040150 (2009).
49. Koven, C. D. et al. The effect of vertically resolved soil biogeochemistry and alternate soil C and N models on C dynamics of CLM4. *Biogeosciences* **10**, 7109–7131 (2013).
50. Plaza, C. et al. Direct observation of permafrost degradation and rapid soil carbon loss in tundra. *Nat. Geosci.* **12**, 627–631 (2019).
51. Parton, W. J., Schimel, D. S., Cole, C. V. & Ojima, D. S. Analysis of factors controlling soil organic matter levels in Great Plains grasslands. *Soil Sci. Soc. Am. J.* **51**, 1173–1179 (1987).
52. Haaf, D., Six, J. & Doetterl, S. Global patterns of geo-ecological controls on the response of soil respiration to warming. *Nat. Clim. Chang.* **11**, 623–627 (2021).

53. Jones, C. D. et al. C4MIP – the Coupled Climate–Carbon Cycle Model Intercomparison Project: experimental protocol for CMIP6. *Geosci. Model Dev.* **9**, 2853–2880 (2016).
54. Bouskill, N. J., Riley, W. J., Zhu, Q., Mekonnen, Z. A. & Grant, R. F. Alaskan carbon-climate feedbacks will be weaker than inferred from short-term experiments. *Nat. Commun.* **11**, 5798 (2020).

[1]Physical and Life Sciences Directorate, Lawrence Livermore National Laboratory, Livermore, CA, USA. [2]Climate and Ecosystem Sciences Division, Lawrence Berkeley National Laboratory, Berkeley, CA, USA. [3]Climate and Global Dynamics Laboratory, National Center for Atmospheric Research, Boulder, CO, USA. [4]Institute of Arctic and Alpine Research, University of Colorado, Boulder, CO, USA. [5]Natural Resource Ecology Laboratory, Colorado State University, Fort Collins, CO, USA. [6]Department of Life and Environmental Sciences, University of California Merced, Merced, CA, USA. [7]Ronin Institute, Montclair, NJ, USA. [8]Department of Ecology and Evolutionary Biology, Yale University, New Haven, CT, USA. [9]Department of Physical Geography and Ecosystem Science, Lund University, Lund, Sweden. [10]Department of Plant Sciences, University of Cambridge, Cambridge, UK. [11]Rocky Mountain Research Station, United States Forest Service, Boise, ID, USA. [12]Climate Change Science Institute and Environmental Sciences Division, Oak Ridge National Laboratory, Oak Ridge, TN, USA. [13]Department of Earth System Science, Stanford University, Stanford, CA, USA. [14]Woods Institute for the Environment and Precourt Institute for Energy, Stanford University, Stanford, CA, USA. ✉e-mail: georgiou1@llnl.gov

Methods

Data sources and processing

The overarching goal of this study was to use observed spatial gradients in soil C stocks—particularly in underlying unprotected (particulate) and protected (mineral-associated) C pools—and their relationships with temperature, to develop benchmarks for ESMs. Although such benchmarks derived from spatial gradients are insufficient for constraining transient responses or making projections (that is, space-for-time assumptions)[31], they do reflect steady-state differences and long-term climatological temperature sensitivities of soil C pools. These observed differences across spatial climate gradients should, in principle, be predicted by dynamical soil C models, and, thus, these benchmarks serve as important tests[4,29]. However, meeting this constraint is not sufficient for ensuring the ability of models to produce accurate projections under global change, and so we urge experimental work that quantifies the transient responses of soil C pools across diverse climates and biomes[8,9,11].

Observationally derived climate and edaphic datasets for all global analyses were used at 0.5 × 0.5° resolution. MAT was estimated from the CRU dataset (version 3.10)[55] and mean annual precipitation from the GPCC dataset[56], both as 30 year annual averages. Land cover was obtained from the MODIS MCD12C1 product[57], and productivity was estimated from the MODIS net primary productivity product[58]. Following Shi et al.[41], soil organic C stocks to 1 m depth were estimated as the mean of Harmonized World Soil Database[59] and SoilGrids[60] maps to reflect a best estimate and uncertainty across data products. Corresponding mineral-associated C stocks and 90% prediction intervals were estimated in Georgiou et al.[33,61] using a machine-learning (random forest) algorithm, and multiple cross-validation approaches were used to provide rigorous assessments of predictability[62,63]. We also note that our conclusions were robust to the selected fractionation method (namely, size and density; Supplementary Fig. 5 and Supplementary Table 5) and reflect a global best estimate and uncertainty given existing observations. However, we encourage further measurements in cooler climates and sandy soils, where the relative contribution of fine particulate organic matter may be more substantial[3,15]. In the present study, we focused our analyses on non-permafrost mineral soils with MAT > 0 °C given data limitations at higher latitudes[33,63]. To exclude soils whose decomposition is limited by water saturation or aridity, we also removed gridcells that contain a coverage of more than 50% peat, defined as the Histosol soil order or Histel suborder, and those that are hyperarid (with an aridity index of <0.05) or receive less than 100 mm yr^{-1} of precipitation. These gridcells were masked in white in all maps (Fig. 3) and were excluded from subsequent analyses.

Global land model output

Model output was sourced from CMIP6 ESMs[34] and three offline biogeochemical testbed models[23] for present-day ('historical') and future projections ('ssp585', or RCP8.5). Only CMIP6 models that reported soil C pool distributions were used in this study. Model details are listed in Supplementary Tables 1–3. Carbon stocks and climate covariates from each model were taken over the historical period as ten year annual averages for C stocks and 30 year annual averages for climate (spanning 2005–2015 and 1985–2015, respectively) to match the observation-based quantities. Specifically, MAT ('tas' for CMIP6 models), mean annual precipitation ('pr') and net primary productivity ('npp') were used from each model. Since the models do not provide depth-resolved C stocks, we used total soil C stocks ('cSoil' for CMIP6 models) in our analyses. Although the depth of soil C in CMIP6 models is not clearly defined, previous studies have compared with 0–1 m integrated soil C stocks[4,43,44]. We believe that this represents the best benchmark on current models and follow this depth correspondence in comparison with the data, but note that any errors in the correspondence with depth could be reduced with future models that are depth-resolved and/or explicitly define a depth interval[4,49].

For the offline models of the biogeochemical testbed (that is, CASA-CNP, MIMICS and CORPSE), mineral-associated (protected) C was estimated by the explicit physicochemically protected pools for MIMICS and CORPSE, and the slowest-cycling (passive) pool for the first-order CASA-CNP model (see Wieder et al.[23] for details on physicochemical protection within the three biogeochemical testbed models). Analogously, for the first-order CMIP6 models, the slowest-cycling C pool ('cSoilSlow') was used to represent mineral-protected C (see 'Model pool interpretability' in the Methods). We note that the CMIP6 model output repository uses the terminology cSoil for total soil C stocks and 'cSoilFast', 'cSoilMedium' and cSoilSlow for the three soil C pools that correspond to the 'active', 'slow', and passive pools, respectively.

Of the ten CMIP6 ESMs that reported soil C pool distributions, only one model constituted a conceptualization that did not align with mineral protection; namely, in TaiESM1, the soil C dynamics were parameterized as a decomposition cascade based on a synthesis of microcosm studies using radio-labelled substrates[64–66]. We thus excluded TaiESM1 from our analyses, and note that the model can be redefined and parameterized for comparison with pool-specific benchmarks in future work. We also emphasize that not all first-order soil C models were formulated as a decomposition cascade based on recalcitrance. Rather, several first-order soil C models implicitly represent key processes by rerouting flows and imposing particular controls (for example, lignin, soil texture and climate) on the formation of select pools[22,24] (see 'Model pool interpretability' in the Methods; Supplementary Fig. 12). To the best of our knowledge, the nine remaining CMIP6 ESMs (namely, ACCESS-ESM1-5, BCC-CSM2-MR, CESM2, CNRM-ESM2-1, E3SM-1-1-ECA, MIROC-ES2L, MRI-ESM2-0, IPSL-CM6A-LR, NorESM2) constitute formulations broadly based on the Century model[51] and its derivatives, for which the slowest-cycling (passive) pool is conceptually aligned with physicochemical protection. Although parameterizations in implemented soil models may have diverged from published values, protected C appears to be defined consistently across the nine remaining CMIP6 ESMs (Supplementary Table 3). To facilitate future benchmarking studies and reduce potential uncertainties, we highly encourage more detailed documentation on parameterizations implemented in soil models within CMIP ESMs.

The protected C pool in each model was then compared with the total soil C for each gridcell globally to calculate the proportion of protected C (Supplementary Fig. 4). The global mean (with 90% CIs) was calculated for each model and in each indicated temperature regime (Fig. 3 and Supplementary Fig. 5). We then calculated the spatially explicit multi-model mean across the ensemble of soil C models (Fig. 3c), as well as the latitudinal means of the observationally derived data product and multi-model ensemble (Fig. 3b). We also quantified changes in soil C pools for each model under an RCP8.5 (or ssp585) scenario by comparing projections from the end of the twenty-first century (2090–2100) with the present day (2005–2015). Results are shown as absolute and relative changes in soil C stocks globally (Supplementary Figs. 6 and 7 and Supplementary Table 4) and across time and latitude (as Hovmöller diagrams; Supplementary Fig. 8).

Model pool interpretability

The comparison of protected C across different model formulations, following the above pool nomenclature, has been proposed in several past studies with first-order models[15,22,23]. We recognize that there are still inherent mismatches between operationally defined, measurable pools of soil organic C fractions and the modelled states that are simulated by different soil biogeochemical models[24,67–69]. Although progress is being made to help bridge this divide[22,45,70,71], the global-scale models that are the focus of this work make assumptions that are broadly consistent with characteristics of mineral-associated and particulate soil C fractions[22–24] (Supplementary Fig. 12).

Indeed, in non-permafrost mineral soils, the formation and composition of the passive pool in select first-order models (for example, in the Century model of Parton et al.[51]) was formulated to resemble the mineral-associated fraction, and mirrors the mathematical representations of physicochemically protected C in several microbially explicit models, including MIMICS and CORPSE[22,23]. Namely, the protected (passive in the first-order models) pool is formed primarily from the microbial (active) pool, where this transfer coefficient is modulated by soil clay and silt content, such that proportionally more C is stored within the protected pool in fine-textured soils[22–24,51,72]. More decomposable (metabolic) litter enters only the microbial (active) pool, whereas structural litter (controlled by lignin content) primarily enters the particulate (slow) pool[23,51]. A small amount of the protected pool forms from direct sorption of the particulate pool[23,73]. Consequently, the C:N ratio of the protected (passive) pool often resembles that of the microbial (active) pool (that is, typically ~11–12 for the protected pool in the Century model[73]), which is consistent with the stoichiometry of mineral-associated organic matter[16,74,75]. By contrast, the C:N ratio of the slow pool is more closely aligned with the stoichiometry of particulate organic matter (that is, ~12–20 in the Century model[73]).

Finally, losses from the protected pool are represented as a first-order process in most soil C models[22,36,45], including the ones presented here, with typical intrinsic turnover times ranging between 75 and 1,000 years, which are broadly consistent with radiocarbon estimates[8,16,18] (see Supplementary Table 3 and Supplementary Fig. 13). Whereas there is heterogeneity within all underlying soil fractions in practice, it is well accepted that mineral-associated organic C is generally slower-cycling (decades to millennia) than particulate organic C (days to decades)[16–18]. Indeed, the intrinsic turnover times for protected (passive) C ranged from 200 to 450 years in all analysed CMIP6 ESMs, except for MIROC-ES2L and MRI-ESM2-0 for which the turnover times were 1,000 years (Supplementary Table 3). By contrast, intrinsic turnover times of the particulate (slow) pool ranged from 5 to 10 years in all analysed CMIP6 ESMs, except for MIROC-ES2L for which the turnover time was 25 years. These intrinsic turnover times are baseline (minimum) pool-specific values, such that environmental modifiers (based on temperature and moisture) further increase the turnover time in most gridcells; for example, by a factor of ~2.5 in temperate forests up to a factor of ~10 in Arctic regions for the Century model[73]. These environmental controls are important when comparing pool-specific turnover times with global radiocarbon data (Supplementary Fig. 14), and future work could estimate the distribution of C ages for each modelled pool across gridcells globally. Leveraging $\Delta^{14}C$ measurements from the International Soil Radiocarbon Database[18,76], and following Shi et al.[41] to convert between turnover time and $\Delta^{14}C$, we show that the protected (passive) pool turnover time within many first-order models is broadly aligned with mean C ages of the mineral-associated fraction (Supplementary Table 3 and Supplementary Figs. 13 and 14). However, future model versions may further improve the correspondence by reducing the intrinsic turnover time of protected C, especially in MIROC-ES2L and MRI-ESM2-0, and strengthening its environmental controls to better match the global distribution of $\Delta^{14}C$ measurements (Supplementary Fig. 14).

By contrast, the turnover time of protected C is fixed at 75 years in CORPSE and ranges from 15 to 80 years in MIMICS based on a dependence on soil texture[23]. We note that the turnover times of MIMICS and CORPSE appear to be biased low compared with radiocarbon data of soil fractions (Supplementary Figs. 13 and 14), which may explain their strong responses under future conditions (Supplementary Figs. 6–8) and suggests that bulk soil C ages may also be too young in these models. In fact, subsequent versions of MIMICS that have yet to be integrated into the global biogeochemical testbed have implemented much longer turnover times of protected C—for instance, ranging from 180 to 1,000 years (that is, increased by a factor of 12.5) in MIMICS-CN[77], and in the C-only MIMICS independently fitted to site-level data at the Reynolds Creek Experimental Watershed[47]. These modifications in subsequent versions of MIMICS have also resulted in much higher proportions of protected C (namely, 50–80%) that are better aligned with observational constraints. Thus, we emphasize that all models, including microbially explicit and first-order formulations, have the opportunity to be falsified or refined in future iterations, but this does not preclude the ability to benchmark them here.

The range of conceptual representations and parameterizations of physicochemical protection across ecosystem to global-scale models (for example, see the schematic in Sulman et al.[22]) presents an urgent need to develop and apply observationally derived constraints. We posit that both the microbially explicit and first-order soil C models in this study (Supplementary Tables 1–3) constitute conceptualizations that are compatible with benchmarking protected soil C to refine future model parameterizations. Although we recognize that there are still inherent uncertainties in the interpretability of modelled pools and operationally defined fractions, we believe that this study represents a valuable benchmark on model pools globally. Observational syntheses show that mineral-associated C is typically an old (Supplementary Fig. 13 and Supplementary Table 3) and large (Fig. 3 and Supplementary Fig. 5) component of total soil C. Thus, the slowest-cycling passive pool in first-order models—which broadly aligns with radiocarbon measurements of mineral-associated C (Supplementary Figs. 13 and 14)—should similarly represent a large fraction of the total soil C pool in mineral soils. Such a correspondence would also improve model performance metrics based on bulk soil C ages[41,42]. Since pool-specific turnover times appear to be broadly aligned with observations, future studies may seek to refine other parameters that strongly affect the proportion of protected C—for example, increasing the fraction of the active pool that flows to the passive pool (Supplementary Figs. 12 and 15) and its mineralogical controls[78]. Such parameters may also be informed by observational estimates of the relative flows of plant- or microbial-derived C to mineral-associated C[15,79]. Ultimately, we contend that benchmarking soil C pool distributions concurrently with radiocarbon ages in future work will present a powerful constraint on soil C dynamics across global models.

Data analysis

We investigated the relationship between soil C stocks (within unprotected and protected C pools) and MAT across the global data product and models. Soil C stocks for each pool were log-transformed and a linear regression was used to reflect a hypothesized exponential relationship with temperature (as in Hartley et al.[29]). To ensure that the observed global patterns were not driven by confounding environmental variables, we used a multiple linear regression to control for net primary productivity, mean annual precipitation and clay and silt content in our analyses. In all cases, the climate and productivity covariates were sourced from their respective model output or data product. Clay and silt content was obtained from the Harmonized World Soil Database[59] as it was not reported for most CMIP6 models. The climatological temperature sensitivity was then calculated from the slope of the log-linear temperature relationship and, following Hartley et al.[29], summarized as the proportional decline in C stocks for every 10 °C (analogous to a climatological Q_{10}, but for C stocks) with corresponding parametric 95% CIs (Supplementary Table 6).

This calculation was then repeated for protected and unprotected soil C pools in the data and models, across all mean temperatures above 0 °C (Fig. 4) and across two underlying temperature regimes, namely cool (<15 °C) and warm (≥15 °C) (Fig. 5 and Supplementary Fig. 9). Soils with mean temperatures below 0 °C were not considered in our analyses due to distinct controls on soil C decomposition (for example, permafrost dynamics[29,48]) and consequent implications on the interpretability of protected pools in first-order models in these regions (Supplementary Fig. 3), as well as higher uncertainties in the data product within this temperature regime[33]. Furthermore, the same

analyses were performed on an observational synthesis[33] (Supplementary Figs. 10 and 11). The general agreement between the observations and data product provides further evidence for the robustness of the reported temperature sensitivity trends between protected and unprotected soil C across climate regimes (Fig. 2c). Differences in climatological temperature sensitivity between protected and unprotected soil C pools, and across the data and models, were deemed statistically significant when the 95% CIs did not overlap (Supplementary Table 6).

Data availability

All data used in this manuscript are fully open-access and available at the references provided. The CMIP6 model output is available from the Earth System Grid Federation at https://esgf-node.llnl.gov/search/cmip6/, the Biogeochemical Testbed model output is available on the Climate Data Gateway at https://doi.org/10.5065/d6nc600w and the observationally derived dataset is available on Zenodo at https://doi.org/10.5281/zenodo.6539765.

Code availability

All code relating to this study is available from the corresponding author on GitHub at https://github.com/katerina-georgiou/global-soilCpools and is archived on Zenodo at https://doi.org/10.5281/zenodo.10515706.

References

55. Harris, I., Jones, P. D., Osborn, T. J. & Lister, D. H. Updated high-resolution grids of monthly climatic observations – the CRU TS3.10 Dataset. *Int. J. Climatol.* **34**, 623–642 (2014).
56. Schneider, U. et al. *GPCC Full Data Reanalysis Version 6.0 at 0.5°: Monthly Land-Surface Precipitation from Rain-Gauges built on GTS-based and Historic Data* (GPCC, 2011); https://doi.org/10.5676/DWD_GPCC/FD_M_V6_050
57. Friedl, M. A. et al. MODIS Collection 5 global land cover: algorithm refinements and characterization of new datasets. *Remote Sens. Environ.* **114**, 168–182 (2010).
58. Zhao, M., Heinsch, F. A., Nemani, R. R. & Running, S. W. Improvements of the MODIS terrestrial gross and net primary production global data set. *Remote Sens. Environ.* **95**, 164–176 (2005).
59. Wieder, W. R., Boehnert, J., Bonan, G. B. & Langseth, M. *Regridded Harmonized World Soil Database v1.2* (ORNL DAAC, 2014); https://doi.org/10.3334/ORNLDAAC/1247
60. Hengl, T. et al. SoilGrids250m: global gridded soil information based on machine learning. *PLoS ONE* https://doi.org/10.1371/journal.pone.0169748 (2017).
61. Georgiou, K. et al. Globally-gridded data for manuscript: global stocks and capacity of mineral-associated soil organic carbon. *Zenodo* https://doi.org/10.5281/zenodo.6539765 (2022)
62. Ploton, P. et al. Spatial validation reveals poor predictive performance of large-scale ecological mapping models. *Nat. Commun.* **11**, 4540 (2020).
63. Meyer, H. & Pebesma, E. Machine learning-based global maps of ecological variables and the challenge of assessing them. *Nat. Commun.* **13**, 2208 (2022).
64. Thornton, P. E. & Rosenbloom, N. A. Ecosystem model spin-up: estimating steady state conditions in a coupled terrestrial carbon and nitrogen cycle model. *Ecol. Modell.* **189**, 25–48 (2005).
65. Lawrence, D. M. et al. Parameterization improvements and functional and structural advances in Version 4 of the Community Land Model. *J. Adv. Model. Earth Syst.* https://doi.org/10.1029/2011MS00045 (2011).
66. Lee, W. L. et al. Taiwan Earth System Model Version 1: description and evaluation of mean state. *Geosci. Model Dev.* **13**, 3887–3904 (2020).
67. Christensen, B. T. in *Evaluation of Soil Organic Matter Models* Vol. 38 (eds Powlson, D. S. et al.) 143–159 (Springer, 1996).
68. Elliot, E. T., Paustian, K. & Frey, S. D. in *Evaluation of Soil Organic Matter Models* Vol. 38 (eds Powlson, D. S. et al.) 161–179 (Springer, 1996).
69. Lehmann, J. & Kleber, M. The contentious nature of soil organic matter. *Nature* **528**, 60–68 (2015).
70. Zhang, Y. et al. Simulating measurable ecosystem carbon and nitrogen dynamics with the mechanistically defined MEMS 2.0 model. *Biogeosciences* **18**, 3147–3171 (2021).
71. Dangal, S. R. S. et al. Improving soil carbon estimates by linking conceptual pools against measurable carbon fractions in the DAYCENT model version 4.5. *J. Adv. Model. Earth Syst.* **14**, e2021MS002622 (2022).
72. Abramoff, R. et al. The Millennial model: in search of measurable pools and transformations for modeling soil carbon in the new century. *Biogeochemistry* **137**, 51–71 (2018).
73. Parton, W. J. & Rasmussen, P. E. Long-term effects of crop management in wheat-fallow: II. CENTURY model simulations. *Soil Sci. Soc. Am. J.* **58**, 530–536 (1994).
74. Cotrufo, M. F., Ranalli, M. G., Haddix, M. L., Six, J. & Lugato, E. Soil carbon storage informed by particulate and mineral-associated organic matter. *Nat. Geosci.* **12**, 989–994 (2019).
75. Rocci, K. S. et al. Aligning theoretical and empirical representations of soil carbon-to-nitrogen stoichiometry with process-based terrestrial biogeochemistry models. *Soil Biol. Biochem.* **189**, 109272 (2024).
76. Lawrence, C. R. et al. An open-source database for the synthesis of soil radiocarbon data: International Soil Radiocarbon Database (ISRaD) version 1.0. *Earth Syst. Sci. Data* **12**, 61–76 (2020).
77. Kyker-Snowman, E., Wieder, W. R., Frey, S. D. & Grandy, A. S. Stoichiometrically coupled carbon and nitrogen cycling in the MIcrobial-MIneral Carbon Stabilization model version 1.0 (MIMICS-CN v1.0). *Geosci. Model Dev.* **13**, 4413–4434 (2020).
78. Georgiou, K. et al. Divergent controls of soil organic carbon between observations and process-based models. *Biogeochemistry* **2**, 775–792 (2021).
79. Angst, G., Mueller, K. E., Nierop, K. G. J. & Simpson, M. J. Plant- or microbial-derived? A review on the molecular composition of stabilized soil organic matter. *Soil Biol. Biochem.* **156**, 108189 (2021).

Acknowledgements

K.G. was supported as a Lawrence Fellow at Lawrence Livermore National Laboratory (LLNL) by the LLNL-LDRD Program under Project No. 21-ERD-045 and 24-LW-053. J.P.-R. and E.W.S. were supported by the US Department of Energy (DOE) Office of Science, Office of Biological and Environmental Research, Genomic Science Program as part of the LLNL Microbes Persist Scientific Focus Area, SCW1632. Work at LLNL was conducted under the auspices of DOE Contract DE-AC52-07NA27344. W.R.W. was supported by National Science Foundation Grants 1926413 and 2031238 and by USDA NIFA-AFRI Grant 2020-67019-31395. C.D.K., W.J.R. and Q.Z. were supported by the US DOE Biological and Environmental Research (BER) Program at LBNL under DOE Contract DE-AC02-05CH11231 through the Regional and Global Model Analysis Program (RUBISCO SFA). N.J.B. was supported by the US DOE BER Early Career Research Program under Contract FP00005182. R.Z.A. and B.N.S. were supported by the US DOE BER at Oak Ridge National Laboratory under DOE Contract DE-AC05-00OR22725. A.A. acknowledges the research environment Biodiversity and Ecosystem Services in a Changing Climate (BECC) at Lund University and funding from the Swedish Research Council (2021-05344).

Author contributions

K.G. conceived and designed the study, based on ideas developed through discussions with C.D.K., W.R.W., W.J.R. and R.B.J. All authors contributed to the study development. K.G., W.R.W., M.D.H. and Q.Z. collected and contributed to the model output. M.D.H., W.J.P., W.R.W., C.D.K., A.A., R.Z.A., D.P. and B.N.S. provided insights on the model

formulations, and J.P.-R., N.J.B., E.W.S. and A.F.A.P. provided feedback on the data analyses. K.G. performed all analyses and wrote the first draft of the paper. All authors contributed to subsequent paper revisions.

Competing interests
The authors declare no competing interests.

Additional information
Supplementary information The online version contains supplementary material available at https://doi.org/10.1038/s41561-024-01384-7.

Correspondence and requests for materials should be addressed to Katerina Georgiou.

Peer review information *Nature Geoscience* thanks Emanuele Lugato and the other, anonymous, reviewer(s) for their contribution to the peer review of this work. Primary Handling Editor: Xujia Jiang, in collaboration with the *Nature Geoscience* team.